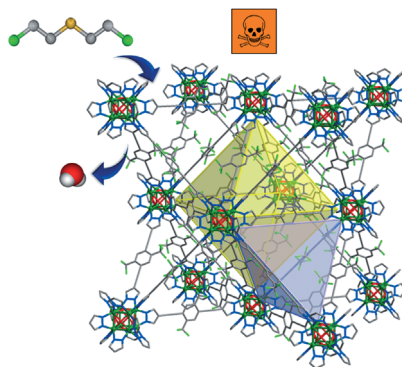# Communications

Metal–Organic Frameworks

N. M. Padial, E. Quartapelle Procopio,
C. Montoro, E. López, J. E. Oltra,
V. Colombo, A. Maspero, N. Masciocchi,
S. Galli, I. Senkovska, S. Kaskel, E. Barea,*
J. A. R. Navarro* ─────── ▮▮▮▮–▮▮▮▮

Highly Hydrophobic Isoreticular Porous
Metal–Organic Frameworks for the
Capture of Harmful Volatile Organic
Compounds

Tunable hydrophobicity: Efficient air filters for the protection against chemical warfare agents might be achieved by surface functionalization of the pores in robust metal–organic frameworks (MOFs) with fluoroalkyl residues and the precise control of their pore size (see picture). These MOFs capture harmful volatile organic compounds even under extremely moist conditions (80% relative humidity).
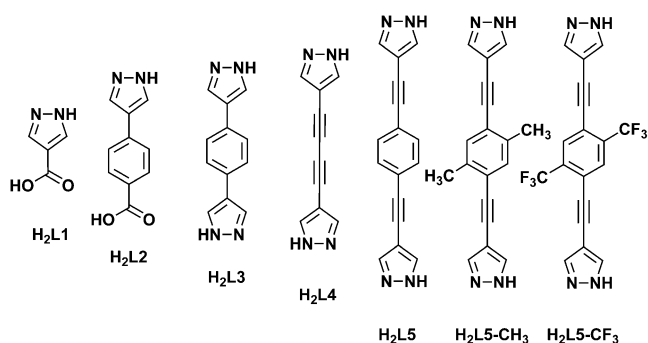
WILEY
ONLINE LIBRARY

1

These are not the final page numbers! ↗↗

Highly Hydrophobic Isoreticular Porous Metal–Organic Frameworks for the Capture of Harmful Volatile Organic Compounds**

Natalia M. Padial, Elsa Quartapelle Procopio, Carmen Montoro, Elena López, J. Enrique Oltra, Valentina Colombo, Angelo Maspero, Norberto Masciocchi, Simona Galli, Irena Senkovska, Stefan Kaskel, Elisa Barea,* and Jorge A. R. Navarro*

The release of toxic pollutants into the environment, which includes oil spills, leaks of harmful industrial products, and the deliberate emission of chemical warfare agents is a risk of growing concern. Worthy of note, oil spill cleanups amount to over 10 billion dollars annually.[1] Remediation of these environmental problems involves the use of large amounts of adsorbents such as sand, activated carbons, or zeolites.[2] However, the effectiveness of such adsorbents is often limited by their affinity to moisture. Consequently, the search for highly hydrophobic porous materials to be used as suitable stopgap of harmful organics spills has become of paramount importance.

In the past years, porous metal–organic frameworks (MOFs) have been extensively studied to explore their possible applications in near future technologies for the safe storage of energetically and environmentally relevant gases.[3,4] The tunable nature of their pores might be beneficial also in cushioning environmental problems caused by the release of harmful volatile organic compounds (VOCs).[5] A remarkable example of the design amenability of MOFs is the well-known isoreticular $[Zn_4OL_3]$ series (L = arene-dicarboxylate), wherein the size and the functionality of the pores can

be modulated in a highly rational and systematic way.[6,7] Nevertheless, the advantageous structural features of this family of MOFs are readily hampered by its high sensitivity to moisture, which limits its practical applications.[8] A similar size-scaling approach has been applied by Lillerud and co-workers on the isoreticular $[Zr_6O_4(OH)_4L_6]$ series,[9] evidencing that a significant improvement in the stability of the material can be achieved with an appropriate combination of dicarboxylate linkers and oxophylic metal fragments.[9] Alternately, it is possible to take advantage of the enhanced stability imparted by polyazolate-containing ligands in combination with borderline metal ions.[10,11] Accordingly, we designed and isolated an isoreticular series of porous MOFs, the pore size and polarity of which was modulated by coupling stiff bi-pyrazolate or mixed pyrazolate/carboxylate linkers (Scheme 1) to Ni^{II} hydroxo clusters acting as 12-connected

[*] N. M. Padial, Dr. E. Quartapelle Procopio, C. Montoro, E. López,
Prof. J. E. Oltra, Dr. E. Barea, Prof. J. A. R. Navarro
Departamentos de Química Inorgánica y Orgánica
Universidad de Granada, Av. Fuentenueva S/N
18071 Granada (Spain)
E-mail: ebaream@ugr.es
jarn@ugr.es
Homepage: http://www.ugr.es/local/jarn

Dr. V. Colombo
Dipartimento di Chimica, Università di Milano
Via Golgi 19, 20133 Milano (Italy)

Dr. A. Maspero, Prof. N. Masciocchi, Dr. S. Galli
Dipartimento di Scienza e Alta Tecnologia
Università dell'Insubria, Via Valleggio 11, 22100 Como (Italy)

Dr. I. Senkovska, Prof. S. Kaskel
Department of Inorganic Chemistry
Dresden University of Technology
Mommsenstrasse 6, 01069 Dresden (Germany)

Scheme 1. Pyrazolate-based ligands used in the synthesis of the $[Ni_8(OH)_4(H_2O)_2(L)_6]_n$ MOFs. $H_2L1 = 1H$-pyrazole-4-carboxylic acid, $H_2L2 = 4$-(1H-pyrazole-4-yl)benzoic acid, $H_2L3 = 4,4'$-benzene-1,4-diylbis(1H-pyrazole), $H_2L4 = 4,4'$-buta-1,3-diyne-1,4-diylbis(1H-pyrazole), $H_2L5 = 4,4'$-(benzene-1,4-diyldiethyne-2,1-diyl)bis(1H-pyrazole), and H_2L5-R (R = methyl, trifluoromethyl).

nodes. This combination yielded the series of $[Ni_8(OH)_4-(H_2O)_2(L)_6]_n$ MOFs (shortened as $[Ni_8(L)_6]$), exhibiting highly porous 3D networks analogous to those recently reported by us (Figure 1).[12,13] Noteworthy, no interpenetration occurred for any of the isolated solids which, therefore, do not suffer from a reduction in the accessibility of voids, as found for some MOFs containing dicarboxylate linkers in primitive cubic lattices,[14] or featuring extremely long (> 2 nm) spacers, in the less common $Fd\bar{3}m$ space group.[15]

In the following, the synthesis, structural and textural characterization of the $[Ni_8(L)_6]$ isoreticular series are pre-

◀◀ **These are not the final page numbers!**
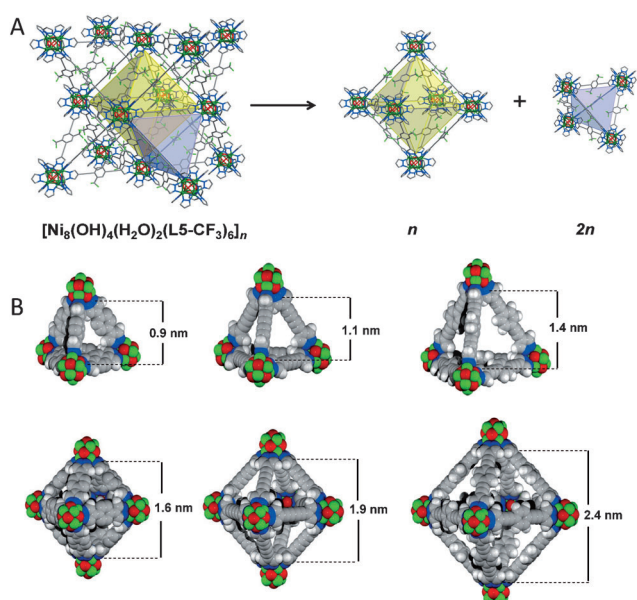
Figure 1. A) The crystal structure of $[Ni_8(OH)_4(H_2O)_2(L5\text{-}CF_3)_6]_n$ viewed as a combination of *n* octahedral (yellow polyhedron) and *2n* tetrahedral (gray polyhedron) cavities. B) View of the tetrahedral (top) and octahedral (bottom) cages found in the crystal structures of $[Ni_8(OH)_4(H_2O)_2(L3)_6]_n$ (left), $[Ni_8(OH)_4(H_2O)_2(L4)_6]_n$ (middle), and $[Ni_8(OH)_4(H_2O)_2(L5)_6]_n$ (right), and the corresponding metric descriptors. **Ni**, **N**, **C**, **O**, **F**, H (white).

Scheme 2. Chemical warfare agent bis(2-chloroethyl)sulphide (BCES, mustard vesicant gas), and the model compound used in our studies, diethylsulphide (DES).

Each Ni^{II} ion is hexacoordinated in a *fac*-NiN_3O_3 fashion and shows intermetallic nonbonding distances close to 3.0 Å. The cubic clusters are connected to 12 adjacent ones by linear *exo*-tetradentate linkers to yield a face-centered cubic (fcu) topology. Their cubic close-packing (ccp) arrangement, analogous to that of the $[Zr_6O_4(OH)_4]$ nodes in the UiO (University of Oslo) series,[9] gives rise to one octahedral and two tetrahedral cavities per MOF formula unit (see Figure 1). A very similar series of MOFs showing the fcu topology and highly tunable sorption performances has been recently reported.[19] As expected from the increasing length of the organic linkers, the unit cell parameters (ranging from 17.17 Å for $[Ni_8(L1)_6]$ to 32.53 Å for $[Ni_8(L5)_6]$), and void volumes (Table 1) of the isolated compounds become progressively larger.

Table 1: Summary of cell volumes, void percentages, and specific surface areas for the $[Ni_8(L)_6]$ series.

Species	V_{cell} [Å³]	Void percentage	S_{BET} [m² g⁻¹]
$[Ni_8(L1)_6]$	5061	34	205
$[Ni_8(L2)_6]$	12503	53	990
$[Ni_8(L3)_6]$	16348	63	1770
$[Ni_8(L4)_6]$	18149	74	1920
$[Ni_8(L5)_6]$	34207	75	2215
$[Ni_8(L5\text{-}CH_3)_6]$	–	–	1985
$[Ni_8(L5\text{-}CF_3)_6]$	34013	64[a]	2195

[a] Underestimated because of -CF_3 disorder in multiple sites.

Chemical stability tests demonstrated that the $[Ni_8(L)_6]$ species survive at room temperature after suspension in basic, yet not in acidic, media for 24 h. As regards the thermal stability, the thermogravimetric (TG) curves show no other thermal event but a steep weight decrease, starting in the range of 300–350 °C and completing near 400 °C, clearly indicating the decomposition of the material (Figure S2). Noteworthy, $[Ni_8(L3)_6]$, the bipyrazolate-containing species with a benzene residue only, exhibits the highest thermal stability and its decomposition starts around 350 °C. Slightly lower decomposition onset temperatures are observed for the remaining materials, which can be reasonably attributed to decarboxylation paths (for L1 and L2) or to the intrinsically lower thermal inertness of alkynes (for L4 and the L5 series).

Variable-temperature XRPD measurements carried out in air[20] demonstrated that all $[Ni_8(L)_6]$ species 1) are thermally stable and rigid, 2) possess permanent porosity, and 3) maintain their thermal stability, together with their framework topology, along consecutive heating–cooling cycles (Figures S6–S8). On the basis of the latter occurrence, it might be proposed that also their adsorption performances are preserved along cycles of thermal activation followed by adsorption.

The accessibility of the pore entrance and surface polarity along the $[Ni_8(L)_6]$ series have been studied by N_2 (77 K) and H_2O (298 K) adsorption experiments (Figures 2 and 3, and Table 1). The N_2 adsorption data indicate that the longer the linker, the higher the porosity, as evidenced by the progressively higher adsorption capacity and specific surface area. Noteworthy, all the MOFs of the series, except $[Ni_8(L5)_6]$ and

sented, together with their possible application for the capture of harmful VOCs (Scheme 2) even in highly competitive, moisture-rich atmosphere (80% relative humidity, RH), which simulates extreme operative conditions.[16]

To synthesize the $[Ni_8(L)_6]$ family, we faced a problem related to the notable strength of the Ni–azolate bonds which, although conferring high stability to the materials, concomitantly induces an extremely fast precipitation and poor solubility,[17] hampering the isolation of single crystals suitable for conventional structural characterization. To facilitate the precipitation of powders with a high degree of crystallinity, Boc-protected pyrazole rings were employed in the case of the bipyrazole linkers (Boc_2L4, Boc_2L5-R; R = H, CH_3, CF_3; Boc = *tert*-butoxycarbonyl), favoring the slow release of the ligand in the reaction medium. X-ray powder diffraction (XRPD) structural analysis was extensively used as a means to characterize the isolated materials (see the Supporting Information).

Noteworthy, all $[Ni_8(L)_6]$ materials crystallize in the cubic $Fm\bar{3}m$ space group and contain ligand-bridged octanuclear $[Ni_8(OH)_4(H_2O)_2]$ clusters, within a 3D porous framework of overall $[Ni_8(\mu_4\text{-}X)_6(\mu_4\text{-}L)_6]$ formulation (X = OH^- or H_2O).[18]
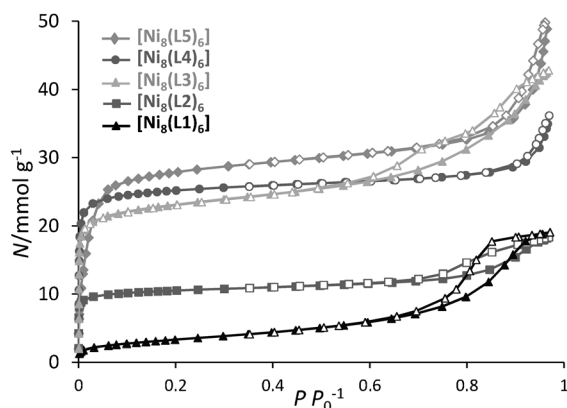
Figure 2. N$_2$ physisorption isotherms (77 K) for the isoreticular [Ni$_8$(L)$_6$] series. Solid symbols denote adsorption, open symbols desorption (PP_0^{-1} = partial pressure).

Figure 3. H$_2$O physisorption isotherms (298 K) for the isoreticular [Ni$_8$(L5-R)$_6$] series and the activated carbon Blücher-101408. Solid symbols denote adsorption, open symbols desorption.

its functionalized analogs, show type I isotherms, characteristic of microporous crystalline solids. The L5-based species feature pores in the mesopore range (2.4 nm wide); therefore, N$_2$ uptake in the low-pressure region is not as steep as for the other compounds. The [Ni$_8$(L5-R)$_6$] (R = CH$_3$, CF$_3$) systems, sharing very similar unit cell parameters, exhibit almost the same uptake of N$_2$ (Figure S3) with just minor differences, suggesting that ligand functionalization does not affect the accessibility of this probe molecule to the porous network, even if it significantly modifies the surface polarity.

As mentioned above, stability towards hydrolysis is a major requirement for practical applications. On the other hand, surface hydrophobicity is also advantageous for applications that involve capture of organic molecules in moist environments. The enhanced stability provided by metal–pyrazolate coordinative bonds can be exemplified by the sensitivity to water of the materials containing mixed pyrazolate/carboxylate-based ligands ([Ni$_8$(L1)$_6$] and [Ni$_8$(L2)$_6$]): after soaking them in water at room temperature for 24 h, a few minor changes are observed in their XRPD patterns (Figure S4); at variance, all the species containing bipyrazolate linkers remain completely unaltered. Measurement of cycles of water adsorption–desorption isotherms at 298 K is a highly valuable tool to evaluate both stability toward hydrolysis and pore surface hydrophobicity of MOFs.[21] Consequently, all the [Ni$_8$(L)$_6$] materials have been studied in this regard (Figure 3 and Figure S5). The behavior of the [Ni$_8$(L)$_6$] species has been compared to that of the highly hydrophobic, commercially available, activated carbon Blücher-101408 (provided by Blücher GmbH), the active species employed in the state-of-the-art Saratoga filtering systems.[22] The comparison shows that the maximum amount of adsorbed water is in line with the pore size and cell volume (see Figure 3 and Figure S5). Noteworthy, while the mixed carboxylate/pyrazolate [Ni$_8$(L1)$_6$] and [Ni$_8$(L2)$_6$] systems are sensitive to moisture, those containing bipyrazolate linkers exhibit a low water affinity as well as a high stability in environmental moisture. Indeed, partial pressures corresponding to the beginning of water vapor condensation into the porous frameworks increase upon extension of the spacer (namely $P/P_o > 0.3$ for [Ni$_8$(L3)$_6$], $P/P_o > 0.5$ for [Ni$_8$(L4)$_6$],
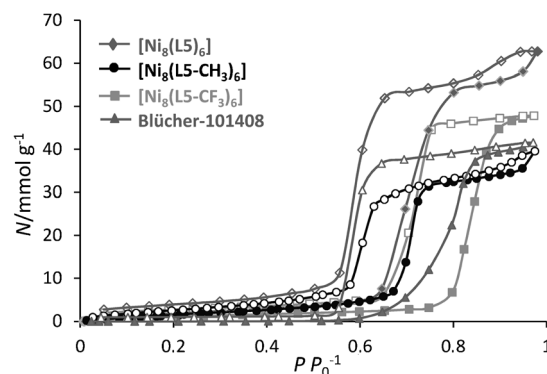
and $P/P_o > 0.6$ for [Ni$_8$(L5)$_6$]) and augment even further upon inclusion of hydrophobic substituents on the benzene ring of H$_2$L5 (namely $P/P_o > 0.65$ for [Ni$_8$(L5-CH$_3$)$_6$], and $P/P_o > 0.80$ for [Ni$_8$(L5-CF$_3$)$_6$]), which is indicative of the increasing hydrophobicity of the frameworks (Figure 3). The relevance of these results is further evidenced if compared to those obtained with prototypical mesoporous MOFs such as MIL-100(Fe) and MIL-101(Cr). Indeed, [Ni$_8$(L5)$_6$] is more hydrophobic than both MIL-100(Fe) and MIL-101(Cr),[21] even if it is slightly less hydrophobic than Blücher-101408, since water vapor enters the structure of the latter only at relative pressures higher than 0.6. Remarkably, while the introduction of methyl groups, as in [Ni$_8$(L5-CH$_3$)$_6$], slightly enhances the hydrophobicity, the functionalization with fluorinated residues, as in [Ni$_8$(L5-CF$_3$)$_6$], gives rise to a highly hydrophobic material, which clearly outperforms Blücher-101408. The low affinity of [Ni$_8$(L5-CF$_3$)$_6$] to moisture is exemplified also by the narrowing of the hysteresis loop, which is in agreement with the narrow pore distribution and is also indicative of easy desorption of the adsorbed moisture. The latter feature further highlights the potential relevance of this MOF under operative humid conditions. In this regard, although Omary and co-workers[5] have shown that the introduction of fluoroalkane residues in a MOF gives rise to a highly hydrophobic material, no report on the systematic variation of the pore size and functionalization to modulate the surface hydrophobicity of the pore can be found in the literature.

The hydrophobic nature of the bipyrazolate [Ni$_8$(L)$_6$] systems prompted us to study their possible use for air purification processes, in which moisture is unavoidably present and acts as a strong competitor with the adsorbates of interest. Consequently, we have investigated the ability of the activated [Ni$_8$(L)$_6$] systems to capture hydrophobic, harmful VOCs under dynamic conditions, in the presence and absence of moisture. As a case of study, we have essayed the performance of these materials for the capture of diethylsulfide (DES, a model of mustard gas, already used by us in previous studies; Scheme 2)[23] from dry and humid Ar/N$_2$ streams. The experiments have been carried out by checking the dynamic weight increase of the activated bipyrazolate [Ni$_8$(L)$_6$] systems as well as of the Blücher-101408 reference material, at room temperature, upon
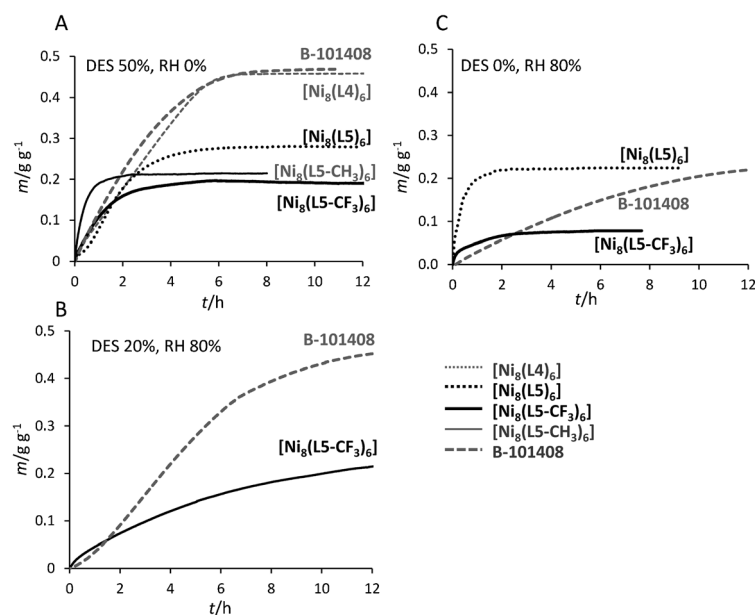
↖↖ These are not the final page numbers!

Figure 4. Dynamic adsorption profiles of DES streams for [Ni$_8$(L4)$_6$], [Ni$_8$(L5)$_6$], [Ni$_8$(L5-CH$_3$)$_6$], and [Ni$_8$(L5-CF$_3$)$_6$], as well as for the Blücher-101408 activated carbon, at 293 K, A) under dry conditions and B) at 80% RH (m = relative weight increase). Dynamic water adsorption at 293 K and 80% RH (C).

exposure to stream of VOCs under dry conditions or in 80% RH (Scheme S1). The experimental results are presented in Figure 4. The results under dry conditions are indicative of rapid incorporation of DES as well as of a high adsorption capacity for all tested materials. Both capacity and kinetics are comparable to those of the Blücher-101408 activated carbon. Indeed, in the case of dry DES streams, the kinetics of the incorporation process is basically independent on the tested material, suggesting that the process depends only on the DES flow, which determines the rate at which the saturation is reached. The best performing materials are [Ni$_8$(L4)$_6$] and Blücher-101408. However, the most significant results have been achieved in the case of strongly competitive moist atmosphere (up to 80% RH) as required under highly demanding operative conditions, for example, in military applications.[16] In this case, it was found that Blücher-101408 as well as [Ni$_8$(L4)$_6$] and [Ni$_8$(L5)$_6$] adsorb significant amounts of water, whereas [Ni$_8$(L5-CF$_3$)$_6$] does not (Figure 4C), as a further proof of its high hydrophobic nature. Indeed, ^{1}HNMR analysis of the adsorbate phase after the adsorption process of DES in highly competitive moist streams reveals that only [Ni$_8$(L5-CF$_3$)$_6$] and Blücher-101408 efficiently capture DES under these conditions (Figure 4B), witnessing that the adsorption of DES by [Ni$_8$(L5-CF$_3$)$_6$] is not affected by the presence of humidity.

Aiming at the evaluation of the strength of the interactions of DES with the studied materials, we also performed pulse gas chromatographic experiments. The variation of the retention volumes (V_g) as a function of temperature, according to the Clausius–Clapeyron-type equation $\Delta H_{ads} = -R\delta$-$(\ln V_g)/\delta(1/T)$ (Figure S6),[24] allows the estimation of the zero-coverage adsorption heats (ΔH_{ads}). On the other hand, the direct relation between the retention volume (V_g) and the

Henry constant (K_H) allows to calculate K_H values at 298 K (Table 2).[23] Noteworthy, the results show a strengthening of DES interactions with the framework on passing from [Ni$_8$(L5)$_6$] to [Ni$_8$(L5-CF$_3$)$_6$], which is indicative of the positive effect of the surface functionalization of the pore with trifluromethane. The values of ΔH_{ads} and K_H for the Blücher-101408 carbon material, although higher, lie in a similar range. These results further support the importance of being able to control the surface hydrophobicity of the adsorbent for the capture of harmful VOCs.

In conclusion, it has been demonstrated that the formation of highly porous 3D frameworks [Ni$_8$(OH)$_4$(H$_2$O)$_2$(L)$_6$]$_n$ is decidedly favored. The strategy shown here reveals not only that it is possible to construct an isoreticular series of MOFs containing azolate ligands, but also that the use of metal–azolate coordinative bonds gives rise to materials with enhanced stability towards hydrolysis. Moreover, the length and functionalization of the linkers impact on the pore size as well as on the fine tuning of the surface polarity. Noteworthy, the incorporation of trifluoroalkyl residues gives rise to a significant increase of hydrophobicity, overcom-

Table 2: Calculated heats of adsorption ΔH_{ads} [kJ mol^{-1}] and Henry constants K_H [cm^3 m^{-2}].

MOF material	VOC	$-\Delta H_{ads}$	K_H[a]
[Ni$_8$(L5)$_6$]	DES	65.87	1.2E+04
[Ni$_8$(L5-CF$_3$)$_6$]	DES	66.51	3.3E+04
Blücher-101408	DES	66.82	1.3E+05

[a] Calculated values at 298 K.

ing the problems associated with the adsorption of harmful VOCs in highly competitive moist environments. Accordingly, the performance in the capture of VOCs along the isoreticular series reported herein might be considered as a first step towards the rational design of MOFs for the capture of harmful VOCs under highly demanding environmental conditions.

[1] C. A. Kontovas, H. N. Psaraftis, N. P. Ventikos, *Mar. Pollut. Bull.* **2010**, *60*, 1455–1466.

[2] M. O. Adebajo, R. L. Frost, J. T. Kloprogge, O. Carmody, S. Kokot, *J. Porous Mater.* **2003**, *10*, 159–170.

[3] K. Sumida, D. L. Rogow, J. A. Mason, T. M. McDonald, E. D. Bloch, Z. R. Herm, T.-H. Bae, J. R. Long, *Chem. Rev.* **2012**, *112*, 724–781.

These are not the final page numbers! ↗↗

[4] B. Wang, A. P. Coté, H. Furukawa, M. O'Keeffe, O. M. Yaghi, *Nature* **2008**, *453*, 207–212.

[5] C. Yang, U. Kaipa, Q. Z. Mather, X. Wang, V. Nesterov, A. F. Venero, M. A. Omary, *J. Am. Chem. Soc.* **2011**, *133*, 18094–18097.

[6] M. Eddaoudi, J. Kim, N. Rosi, D. Vodak, J. Wachter, M. O'Keeffe, O. M. Yaghi, *Science* **2002**, *295*, 469–472.

[7] H. Furukawa, N. Ko, Y. B. Go, N. Aratani, S. B. Choi, E. Choi, A. Ö. Yazaydin, R. Q. Snurr, M. O'Keeffe, J. Kim, O. M. Yaghi, *Science* **2010**, *329*, 424–428.

[8] J. A. Greathouse, M. D. Allendorf, *J. Am. Chem. Soc.* **2006**, *128*, 10678–10679.

[9] J. H. Cavka, S. Jakobsen, U. Olsbye, N. Guillou, C. Lamberti, S. Bordiga, K. P. Lillerud, *J. Am. Chem. Soc.* **2008**, *130*, 13850–13851.

[10] V. Colombo, S. Galli, H. J. Choi, G. D. Han, A. Maspero, G. Palmisano, N. Masciocchi, J. R. Long, *Chem. Sci.* **2011**, *2*, 1311–1319.

[11] M. Tonigold, Y. Lu, A. Mavrandonakis, A. Puls, R. Staudt, J. Möllmer, J. Sauer, D. Volkmer, *Chem. Eur. J.* **2011**, *17*, 8671–8695.

[12] N. Masciocchi, S. Galli, V. Colombo, A. Maspero, G. Palmisano, B. Seyyedi, C. Lamberti, S. Bordiga, *J. Am. Chem. Soc.* **2010**, *132*, 7902–7904.

[13] E. Quartapelle Procopio, S. Rojas, N. Padial, S. Galli, N. Masciocchi, F. Linares, D. Miguel, J. E. Oltra, J. A. R. Navarro, E. Barea, *Chem. Commun.* **2011**, *47*, 11751–11753.

[14] a) J. Hafizovic, M. Bjørgen, U. Olsbye, P. D. C. Dietzel, S. Bordiga, C. Prestipino, C. Lamberti, K. P. Lillerud, *J. Am. Chem. Soc.* **2007**, *129*, 3612–3620; b) J. Kim, S. T. Yang, S. B. Choi, J. Sim, J. Kim, W. S. Ahn, *J. Mater. Chem.* **2011**, *21*, 3070–3076, and references therein.

[15] A. Schaate, P. Roy, T. Preuße, S. J. Lohmeier, A. Godt, P. Behrens, *Chem. Eur. J.* **2011**, *17*, 9320–9325.

[16] M. Tomizuka, H. A. Hakeel, C. Atkeson, L. Brosseau, Z. Frund, D. Jan, S. Jayaraman, L. Kobayashi, D. Newman, A. Sanderson, R. P. Schaudies in *Soldier protective clothing and equipment: feasibility of chemical testing using a fully articulated robotic mannequin*, National Academies Press, Washington, DC, **2007**, pp. 21–47.

[17] This occurrence limits self-healing processes during crystal growth by equilibrating with the solution environment.

[18] As observed for other $[Ni_8(\mu_2\text{-X})_6]$ clusters, the OH^- and H_2O moieties statistically occupy, in a 2:1 ratio, the X-sites. See for example, V. Ovcharenko, E. Fursova, G. Romanenko, I. Eremenko, E. Tretyakov, V. Ikorskii, *Inorg. Chem.* **2006**, *45*, 5338–5350.

[19] These species show the same statistical disorder when asymmetric ligands similar to our pyrazolate/carboxylate ones L1 and L2 are employed. D.-X. Xue, A. J. Cairns, Y. Belmabkhout, L. Wojtas, Y. Liu, M. H. Alkordi, M. Eddaoudi, *J. Am. Chem. Soc.* **2013**, *135*, 7660–7667.

[20] Two sets of experiments were carried out: 1) progressive heating up to decomposition; 2) heating–cooling cycles in the 50–200 °C range.

[21] P. Küsgens, M. Rose, I. Senkovska, H. Fröde, A. Henschel, S. Sieglea, S. Kaskel, *Microporous Mesoporous Mater.* **2009**, *120*, 325–330.

[22] http://www.bluecher.com/en/.

[23] C. Montoro, F. Linares, E. Quartapelle Procopio, I. Senkovska, S. Kaskel, S. Galli, N. Masciocchi, E. Barea, J. A. R. Navarro, *J. Am. Chem. Soc.* **2011**, *133*, 11888–11891.

[24] G. Guiochon, A. Felinger, A. M. Katti, D. G. Shirazi in *Fundamentals of Preparative and Nonlinear Chromatography*, Elsevier, Amsterdam, **2006**.

↖↖ These are not the final page numbers!